Digital Signal Recovery with Transmitter Nonlinear State Tracking for Satellite Communications

Chen, Qingyue; Li, Yunfeng; Jalili, Feridoon; Wang, Zhugang ; Jensen, Ole Kiel; Pedersen, Gert Frølund; Shen, Ming

Published in:
I E E E Transactions on Circuits and Systems. Part 2: Express Briefs

DOI (link to publication from Publisher):
10.1109/TCSII.2022.3181785

Publication date:
2022

Document Version
Accepted author manuscript, peer reviewed version

Digital Signal Recovery with Transmitter Nonlinear State Tracking for Satellite Communications

Qingyue Chen, Yunfeng Li, Feridoon Jalili, Zhugang Wang, Ole Kiel Jensen, Gert Frølund Pedersen, *Senior Member, IEEE,* Ming Shen, *Senior Member, IEEE*

***Abstract*—This brief proposes a digital signal recovery (DSR) method to compensate the nonlinear distortion introduced by power amplifiers (PAs) under dynamic nonlinear operating states. Unlike conventional PA linearization methods that extract the nonlinearity based on the baseband I/Q PA input and output signal samples, the proposed method attempts to derive the memory polynomial (MP) model parameters based on PA operating states using a deep neural network (DNN). This method allows the receiver to achieve DSR by tracking the operating states of the PA effectively with a few telemetry data. Validation results from simulations and experiments based on a GaN PA operating at 3.5 GHz reveal that the proposed method can maintain satisfactory DSR performance in terms of adjacent channel power ratio (ACPR) and error vector magnitude (EVM) while the transmitter PA is operating with fluctuating average input/output power, supply voltage, and bias voltage. The training data size and time are further reduced by using a transfer learning (TL) approach.**

***Index Terms*—Operating states tracking, deep neural network, digital signal recovery, power amplifier, satellite communications.**

I. Introduction

In order to enhance the efficiency of space-borne power amplifiers (PAs) while maintaining good linearity of the transmitted signal, PA linearization techniques such as digital pre-distortion (DPD) [1]–[6] methods based on the memory polynomial (MP) model have been widely used. Owing to the fact that it neither increases complexity nor power consumption of the satellite system, digital post-distortion (DPoD) [7]–[9] methods which correct the nonlinear distortion of the signal received at the receiver side is more appealing for satellite to ground communications. The premise of the DPoD methods is that the PA working conditions need to be maintained to obtain a stable operating state. Although satellite transmission systems are usually designed with high robustness, there could be small-scale fluctuations in signal levels and power supplies due to the harshness of the irradiation environment [10]. These small fluctuations could cause significant variations in the nonlinearity of the PA and hence adaptive model updating is required, which is challenging for MP based DPoD methods.

Q. Chen and Y. Li are with the National Space Science Center, Chinese Academy of Sciences, Beijing, 100190 China, also with the University of Chinese Academy of Sciences, Beijing, 100049 China, also with the Department of the Electronic Systems, Aalborg University, Aalborg, 9220 Denmark (e-mail: qich@es.aau.dk; yli@es.aau.dk).

Z. Wang is with the National Space Science Center, Chinese Academy of Sciences, Beijing, 100190 China (e-mail: wangzg@nssc.ac.cn).

F. Jalili, O. Jensen, G. Pedersen, and M. Shen are with the Department of the Electronic Systems, Aalborg University, Aalborg, 9220 Denmark (e-mail: fja@es.aau.dk; okj@es.aau.dk; gfp@es.aau.dk; mish@es.aau.dk.

Manuscript received xxxx xx, xxxx; revised xxxx xx, xxxx.

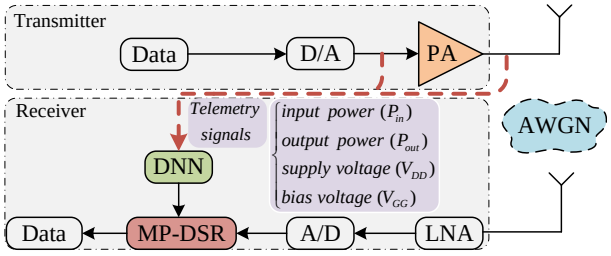

Fig. 1: System architecture of the proposed method.

Given an envelope detection method to switch to three different Sub-DPD modules, the authors of [11] achieved adaptive tracking of different input power levels. As mentioned in [12], the power adaptive decomposed vector rotation method is proposed to adjust the DPD coefficients, so that the PA dynamic behavior caused by power variation can be effectively compensated. These methods, however, are for DPD rather than DPoD, and only power variations were taken into account, while the bias and supply voltage variations are not considered.

Nowadays, deep learning (DL) has demonstrated its powerful ability to deal with linearization challenges in PAs. The methods based on deep neural networks (DNN) [13], [14] and convolutional neural networks (CNN) [15] simulate the memory effects of PAs by adding delayed items in the input layer. The long short-term memory (LSTM) assisted methods [16], [17] obtain memory effect compensation by extracting the sequential characteristics of adjacent I/Q samples. DNN-based digital signal recovery (DNN-DSR) [13] is a novel method for efficient operation of space-borne PAs by correcting nonlinear distortion signals received by ground stations. To deal with the situation of updating the beamforming direction at any time, [18] has adopted a unified DNN-DPD method trained with combined datasets of different beamforming directions. [19] proposed polynomial-assisted DNN that embeds conventional polynomial basis functions into DNN structure to enhance the behavior modeling capability of PAs, yielding better performance with only a small number of network parameters. Whereas, these I/Q based methods can barely cope with dynamic operating states and obtain consistent linearity.

In this brief, we propose a DNN-aided MP digital signal recovery (MP-DSR) method as illustrated in Fig. 1. Different from conventional linearization methods based on I/Q samples, the proposed method can track PA operating states and extract the corresponding MP correction parameters based on state monitoring data (i.e., telemetry signals). Although the PA

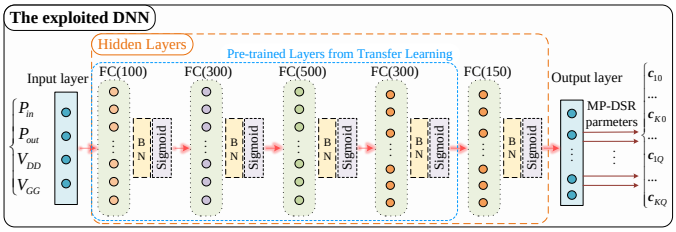

Fig. 2: Structure of the exploited DNN.

operates in different states due to fluctuating average input power (P_{in}), supply voltage (V_{DD}), and bias voltage (V_{GG}), these working conditions of the circuit system can be observed from the ground stations, and usually, the parameters vary within a certain range. Off-line training is performed with the datasets comprised of these variables, based on which the corresponding MP-DSR parameters can be generated as the operating states of the circuit change. Thus, the proposed method deployed at ground stations can enhance the power efficiency of the circuit by compensating for its nonlinearity, even under varying working conditions. The proposed method combines the conventional mature MP linearization technique to ensure the interpretability and reliability of the DL model.

II. Proposed DNN-aided MP-DSR method

A. Nonlinear PA model

At the receiver, we mainly consider compensating the nonlinear distortion and memory effects caused by high-efficiency PAs. The nonlinear PA can be accurately modeled using the Volterra series. However, since its number of parameters increases exponentially with memory depth and the order of nonlinearity, a simplified form of MP is often applied in actual projects, which can be expressed as

$$y(n) = \sum_{k=1}^{K} \sum_{q=0}^{Q} c_{k,q} x(n-q)|x(n-q)|^{k-1}, \tag{1}$$

where K and $Q+1$ represent the order of nonlinearity and the depth of memory, respectively. $c_{k,q}$ denotes the complex coefficient of the MP model. Generally, memory effects of PAs based on GaN/GaAs are supposed to originate from self-heating, dynamic trapping, and biasing circuits.

The linearization solutions based on the model as shown in formula (1) achieve the overall linearization of the received signal by assigning different amplitudes with different gains. We define the new series as $\boldsymbol{u}_{kq} = [u_{kq}(0), ..., u_{kq}(N-1)]^{\mathrm{T}}$, whose elements are $u_{kq}(n) = x(n-q)|x(n-q)|^{k-1}$. The value of N is set to 100,000, representing the PA input and output collected for each operating state, for the following simulations and experiments section. Therefore, formula (1) can be abbreviated as $\boldsymbol{y} = \boldsymbol{U}\boldsymbol{c}_{ex}$, where $\boldsymbol{U} = [\boldsymbol{u}_{10}, ..., \boldsymbol{u}_{K0}, ..., \boldsymbol{u}_{1Q}, ..., \boldsymbol{u}_{KQ}]$. $\boldsymbol{c}_{ex}$ represents the expected complex coefficients and can be estimated as $\boldsymbol{c}_{es}$ using the least square (LS) algorithm $\boldsymbol{c}_{es} = (\boldsymbol{U}^H\boldsymbol{U})^{-1}\boldsymbol{U}^H\boldsymbol{y}$, where $\boldsymbol{y} = [y(0), y(1), ..., y(N-2), y(N-1)]^{\mathrm{T}}$ and $\boldsymbol{c}_{es} = [c_{10}, ..., c_{K0}, ..., c_{1Q}, ..., c_{KQ}]^{\mathrm{T}}$. By swapping the input and output signals, the parameters of the inverse function of the PA can then be obtained for linearization.

B. Proposed DNN-aided MP-DSR method

The conventional MP-DSR method utilizes a set of fixed parameters corresponding to a specific operating state to do the overall linearization. As will be seen in the simulations and experiments section, any possible fluctuations can deteriorate the performance of signal recovery, since these MP-DSR parameters are dependent on the working conditions of the PA. Under different working conditions of fluctuating P_{in}, V_{DD}, and V_{GG}, the operating state and the corresponding nonlinearity of the PA will change. Nevertheless, due to complex physical characteristics, it is not feasible to derive its analytic expression based on the monitoring data. Hence, most of the existing models fit the Volterra series or MP by input and output I/Q samples of the PA. Whereas, DNN can theoretically fit any arbitrary nonlinear functions according to the universal approximation theorem [20]. Therefore, we attempt to apply a DNN module to extract the nonlinear behavior of the PA based on the monitoring data. Specifically, the MP-DSR parameters of the PA are generated as the operating state changes. And it is worth pointing out that these parameters can compensate memory effects of PAs because the MP model has already taken them into account.

In addition to the three input variables, we also consider whether the PA is working correctly by including the average output power (P_{out}) as an input element. These four working conditions are the properties of the circuit system that we are most concerned about. Taking into account the performance and computational complexity, the network structure is designed as shown in Fig. 2. The proposed method consists of two processes, off-line training and on-line application. In the off-line training process, the proposed method can assign corresponding MP-DSR parameters to each operating state of the PA. This allows the DNN to learn enough about the time-varying PA states throughout the fluctuation range. The output of the DNN can be written as

$$\boldsymbol{C} = f^{DNN}(P_{in}, P_{out}, V_{DD}, V_{GG}), \tag{2}$$

where $f^{DNN}(\cdot)$ denotes the DNN model including weights, biases, and activation function. In the on-line application phase, the new monitored telemetry signal are $({P_{in}}', {P_{out}}', {V_{DD}}', {V_{GG}}')$, and the near-optimal MP-DSR parameters can be acquired, which can be expressed as

$$\boldsymbol{C}' = f^{DNN}({P_{in}}', {P_{out}}', {V_{DD}}', {V_{GG}}'). \tag{3}$$

Since the network has been adequately trained off-line, the new operating states can mostly be handled. By doing so, the linearization correction can be implemented at the receiver without occupying space-borne resources.

The input layer ($\boldsymbol{p}_i$) of the exploited DNN depicted in Fig. 2 consists of inputs $P_{in}, P_{out}, V_{DD}, V_{GG}$, and they are fed to the following hidden layers, each of which consists of a fully connected (FC) layer and a batch normalization (BN) layer. The output of the i-th FC layer can be expressed as $\boldsymbol{v}_i = \boldsymbol{w}_i\boldsymbol{u}_i + \boldsymbol{b}_i$, where $\boldsymbol{w}_i$ and $\boldsymbol{b}_i$ are the weights and biases, respectively. $\boldsymbol{u}_i$ is the input of the i-th FC layer. The i-th BN layer is given as

$$\hat{\boldsymbol{v}}_i = \boldsymbol{\gamma}\frac{\boldsymbol{v}_i - E[\boldsymbol{v}_i]}{\sqrt{Var[\boldsymbol{v}_i] + \boldsymbol{\varepsilon}}} + \boldsymbol{\beta}, \tag{4}$$

where $\boldsymbol{v}_i$ and $\hat{\boldsymbol{v}}_i$ represent the input and output of the i-th BN layer, respectively. $\boldsymbol{\gamma}$ and $\boldsymbol{\beta}$, which denote the new mean and variance of the input data, are the scaling and shifting parameters, respectively. Besides, $\boldsymbol{\varepsilon}$ is set to 0.001 to prevent the denominator from being zero. The BN layer enables the DNN to quickly and steadily respond to signals with dynamic changes by recentering and rescaling the input data.

Convergence acceleration is achieved by using the Sigmoid activation function which is defined as $F_{Sigmoid}(\hat{\boldsymbol{v}}_i) = 1/1 + e^{-\hat{\boldsymbol{v}}_i}$, where $\hat{\boldsymbol{v}}_i$ is the input of the i-th Sigmoid function. Finally, the outputs of hidden layers are fed to the output layer. The output layer $\boldsymbol{c}_{p_i} = [\boldsymbol{c}_{10}, ..., \boldsymbol{c}_{K0}, ..., \boldsymbol{c}_{1Q}, ..., \boldsymbol{c}_{KQ}]$ consists of the parameters of the LS solution of the MP-DSR method. $\boldsymbol{c}_{kq}$=$[\mathrm{Re}(c_{k,q}), \mathrm{Im}(c_{k,q})]$ indicates the real and imaginary parts of the correction parameter. Therefore, the data format of the training data and the labels are set to $\boldsymbol{P} = [\boldsymbol{p}_1, \boldsymbol{p}_2, ..., \boldsymbol{p}_N]^{\mathrm{T}}$ and $\boldsymbol{c}_P = [\boldsymbol{c}_{p_1}, \boldsymbol{c}_{p_2}, ..., \boldsymbol{c}_{p_N}]^{\mathrm{T}}$, respectively. Besides, the mean squared error (MSE) is chosen as the loss function of the back propagation (BP) algorithm:

$$MSE = \frac{1}{M}\sum_{i=1}^{M}\left(O^{(m)} - T^{(m)}\right)^2, \tag{5}$$

where $O^{(m)}$ and $T^{(m)}$ represent the observed value and the true value, respectively. M denotes the batch size and the superscript (m) is the index of the m-th training sample. Furthermore, the adaptive moment estimation (Adam) algorithm is selected as the optimizer. It is noteworthy that the scale of the DNN is not small but would not be an issue since the computational resources of the ground station are very powerful and low cost.

III. Simulations and Experiments

A. Simulations validation and results

In order to obtain sufficient data quickly and accurately, we utilize Advanced Design System (ADS) from Keysight Technologies to build an equivalent circuit based on the layout and schematic details given in the CGH40006P PA evaluation board datasheet [21]. CGH40006P is an unmatched, gallium nitride (GaN) high electron mobility transistor (HEMT). The baseband LTE OFDM signal with a bandwidth of 10 MHz operating at C-band, 3.5 GHz, is collected from a signal generator (R&S SMBV100A) and then uploaded to the PA input of ADS. As recommended by the datasheet, when the P_{in}, V_{DD}, and V_{GG} are set to 30 dBm, 28 V, and -2.76 V, respectively, the PA can operate in the primary state (S0) and offer a high drain efficiency of 38%. Assume that these three preset values may fluctuate within a small range, from 29.1 to 31.0 dBm, 27.6 to 28.5 V, and -2.80 to -2.72 V, respectively. With granularities of 0.1 dBm, 0.1 V, and 0.01 V for P_{in}, V_{DD}, and V_{GG} respectively, 2000 sets of PA input and output I/Q data with different working conditions are collected. The memory depth and nonlinearity order are both set to 5. Then the MP-DSR parameters corresponding to each PA operating state are obtained by using the LS algorithm and stored as labels for the proposed network. In these operating states, the PA operates in the vicinity of the saturation region and maintains high drain efficiency, which can make full use of the power resources of the satellite. After the network is trained, testing is conducted on 20 new datasets randomly selected within the fluctuation range of the three input conditions. Note that, these data are not seen by the model during the training phase. Hence, it can effectively handle the nonlinear distortion under dynamic operating states.

For comparison, we also test two other methods, namely the Fixed-MP-DSR method and the Unified-DNN-DSR method. Under the S0 state, the experimental input and output I/Q components of the PA are collected, and the parameters of the Fixed-MP-DSR method are obtained by the LS algorithm. Under fluctuating working conditions, this set of MP parameters is used to correct the distorted signal in all states. In addition, the experimental output I/Q samples of all operating states are sequentially concatenated into a long signal and the same input I/Q samples are adopted as the labels of the Unified-DNN. After joint training, the parameters of the Unified-DNN-DSR method can be acquired. Furthermore, under ideal conditions (assuming timely tracking of state changes), the optimal performance achieved by the MP-DSR is used as a benchmark, which we call the perfect MP-DSR, adopting the MP parameters derived from each operating state. Note that the memory depth and nonlinear order of both Fixed-MP-DSR method and perfect MP-DSR are set to 5, the same as those in the proposed method, for a fair comparison. Both the proposed method and the Unified-DNN-DSR method apply 10-fold cross-validation to improve the generalization ability of the exploited DNN and avoid overfitting. The training, validation, and testing of these two methods are implemented using TensorFlow 1.14 via the Keras API in Python 3.7.6.

Then, these DSR methods are performed on the distorted signals from different operating states. Under different operating states (S1-S20), the EVM performance is illustrated in Fig. 3(a). As can be observed, the proposed method offers superior linearization capabilities compared to the Fixed-MP-DSR method and Unified-DNN-DSR method, and the EVM performance is almost the same as that of the perfect MP-DSR. The MP parameters obtained by the Fixed-MP-DSR method can cover the low P_{ins}, P_{outs}, V_{DDs}, V_{GGs} (S1-S10) but not the high P_{ins}, P_{outs}, V_{DDs}, V_{GGs} (S11-S20). The S11-S20 are the most valuable regions where the PA operates with high efficiency. Therefore, the proposed method outperforms the Fixed-MP-DSR method in EVM by approximately 0.6% in the S11-S20 states. The Unified-DNN-DSR method achieves its best EVM performance at the S10 state and is far worse than the proposed method in the entire test interval.

Assuming that perfect channel equalization has been employed, the received signal will include distorted signals and AWGN. We select a highly nonlinear state operating near state S18 for noise robustness analysis. Fig. 3(b) demonstrates that the proposed method appears more robust to AWGN than others. When the EVM is required to be 5%, the SNR performance can be improved by approximately 4.3 dB using the proposed method, which demonstrates a saving of 4.3 dB in transmitted power while maintaining a consistent EVM. Thus, the power efficiency of the satellite can be greatly increased. Particularly, when the SNR is 30 dB, the proposed method can acquire approximately 0.84% and 2.39%

TABLE I: Working conditions and drain efficiencies of the PA of 20 test datasets.

States	S1	S2	S3	S4	S5	S6	S7	S8	S9	S10	S11	S12	S13	S14	S15	S16	S17	S18	S19	S20
P_{in} (dBm)	29.10	29.18	29.27	29.40	29.49	29.58	29.66	29.78	29.90	29.99	30.07	30.18	30.26	30.39	30.50	30.59	30.65	30.78	30.89	30.98
P_{out} (dBm)	36.25	36.29	36.34	36.43	36.49	36.53	36.57	36.64	36.73	36.77	36.82	36.89	36.94	37.02	37.10	37.15	37.17	37.26	37.33	37.38
V_{DD} (V)	27.50	27.54	27.59	27.63	27.68	27.73	27.78	27.82	27.89	27.92	27.97	28.04	28.06	28.12	28.17	28.23	28.29	28.33	28.38	28.46
V_{GG} (V)	-2.800	-2.798	-2.792	-2.787	-2.783	-2.780	-2.777	-2.771	-2.768	-2.762	-2.760	-2.759	-2.752	-2.748	-2.743	-2.740	-2.736	-2.731	-2.727	-2.722
Efficiency (%)	35.11	35.32	35.60	35.88	36.22	36.53	36.79	37.07	37.38	37.64	37.99	38.32	38.65	38.94	39.20	39.51	39.83	40.11	40.42	40.78

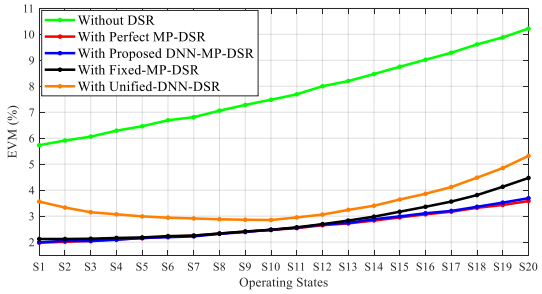

(a) Relation between the EVM and operating states.

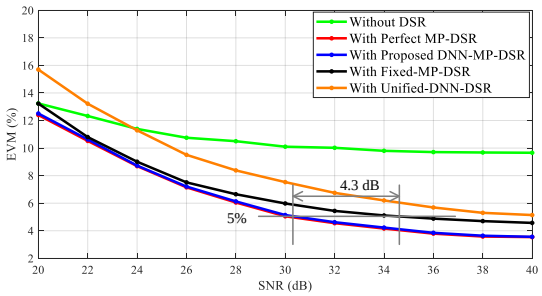

(b) EVM versus SNR under the AWGN channel @ S18.

Fig. 3: EVM performance versus operating states and SNR.

improvement of the EVM, compared with the Fixed-MP-DSR method and the Unified-DNN-DSR method, respectively. This can significantly improve the quality of the received signal.

B. Experimental validation and results

The proposed method is further validated by experiments using the setup illustrated in Fig. 4. The baseband LTE OFDM signal with a PAPR of 10.06 dB and a bandwidth of 10MHz is generated by MATLAB and then uploaded to the signal generator to transmit radio frequency signals operating at C-band, 3.5 GHz. Then, we add a pre-amplifier (MILMEGA AS0204-7R) to drive the main CGH40006P PA. The distorted signal is captured by a signal analyzer (R&S FSQ26) and processed with MATLAB. In the experiment, we still focus on the dynamic variations of P_{in}, V_{GG}, and V_{DD} with granularities of 0.1 dBm, 0.5 V, and 0.02 V, respectively. Then we can collect 300 datasets for training and validation. In addition, 20 datasets are collected to test whether the well-trained DNN performs effectively for actual situations with multi-condition variations. These working conditions and the drain efficiency of the PA are shown in Table I. As in the simulation validation, the memory depth and nonlinearity order are set to 5 for MP-DSR parameter calculation. The parameters of the four hidden layers (pre-trained layers, as demonstrated in Fig. 2) obtained from the simulations validation are transferred to the DNN used in the experimental validation as initial values. Since the

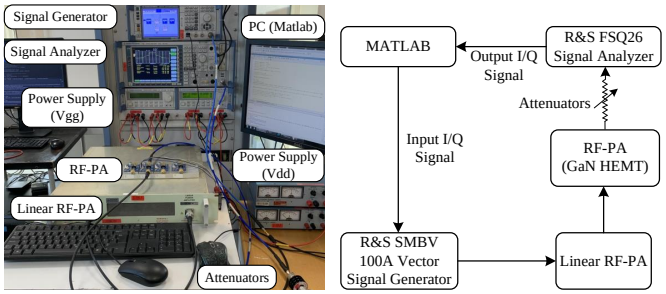

(a) Experimental setup. (b) Schematic diagram.

Fig. 4: Experimental setup and its schematic diagram.

TABLE II: Comparison with existing methods

States	S3		S10		S18	
Scheme	ACPR	EVM	ACPR	EVM	ACPR	EVM
Original signal	-46.35 dBc	-	-46.35 dBc	-	-46.35 dBc	-
Without DSR	-30.13 dBc	9.37%	-28.50 dBc	11.16%	-26.80 dBc	13.45%
Perfect MP-DSR	-44.59 dBc	1.43%	-44.30 dBc	1.47%	-43.44 dBc	1.56%
DNN-MP-DSR	**-44.51 dBc**	**1.45%**	**-44.28 dBc**	**1.47%**	**-43.47 dBc**	**1.55%**
Fixed-MP-DSR	-43.87 dBc	1.58%	-44.30 dBc	1.48%	-40.70 dBc	2.22%
Unified-DNN-DSR	-41.55 dBc	2.16%	-42.82 dBc	2.04%	-37.71 dBc	3.75%

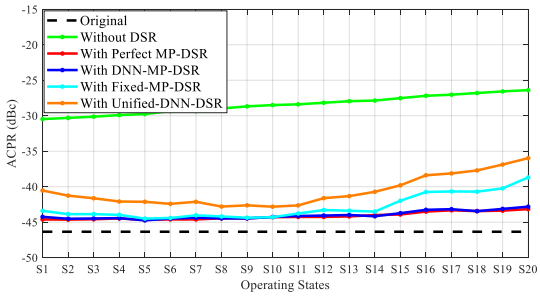

Fig. 5: Measured ACPR performance of different methods.

fabrication tolerance brought about differences between simulation and experiment, an additional hidden layer was added to further update the DNN. Employing such a simulation-to-experiment transfer learning (TL)-assisted approach saves the amount of experimental data as well as 45% of the training time, compared to training from scratch.

The nonlinearity of the 20 states under test is getting stronger, among which S10 is close to the primary state (30 dBm of P_{in}, 28 V of V_{DD}, and -2.76 V of V_{GG}). For all testing operating states, due to the deviation of data collection, the experimental results will fluctuate but trend to satisfactorily match the simulations. The proposed DNN-MP-DSR method can better correct nonlinear distortion than the other two methods and the EVM results have been completely analyzed in detail in the simulation validation and results section. Here S3, S10, and S18 states are chosen as examples to demonstrate the proposed method cases with low, medium, and high nonlinearities. Comparison with other methods in

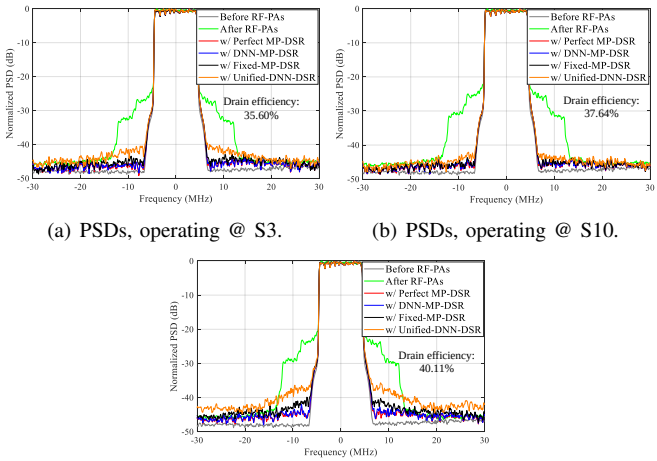

(a) PSDs, operating @ S3. (b) PSDs, operating @ S10.

(c) PSDs, operating @ S18.

Fig. 6: Measured PSDs of different DSR methods.

terms of EVM and adjacent channel power ratio (ACPR) is shown in Table II. The results of the proposed method is almost the same as the perfect MP-DSR results. As for EVM performance, especially for the S18 state, the proposed method outperforms the Fixed-MP-DSR method and the Unified-DNN-DSR method by 0.67% and 2.20%, respectively.

The ACPR performance under different methods are depicted in Fig. 5. The improvements in ACPR using the proposed DNN-MP-DSR method are approximately 0.5-3.0 dB and 1.4-5.7 dB better than the Fixed-MP-DSR method and the Unified-DNN-DSR method, respectively. When the PA operates near the S3, S10, and S18 states, the power spectrum densities (PSDs) under different methods are indicated in Fig. 6, respectively. It can be seen that under these working conditions, the PA operates in different states with low, medium, and high nonlinearities. The ACPR performance of the perfect MP-DSR and the proposed DNN-MP-DSR method are similar and gratifying, dramatically improving the expansion phenomenon of out-of-band spectrum. Other methods can only achieve good results under operating states with medium efficiency (e.g., S10). As S3 and S18 are relatively marginal, the performance gap among various methods is obvious.

IV. Conclusion

In this brief, we proposed a digital signal recovery (DSR) method that incorporates the conventional memory polynomial model (MP-DSR) with deep learning to tackle the nonlinear distortion caused by PAs in satellite communications. By making full use of the telemetry monitoring data of the space-borne PA, a set of MP-DSR parameters can be generated by the trained deep neural network for correction of nonlinear distortion even when the PA is under dynamic operating states with varying input power levels, bias voltages, and supply voltages. Simulation and experimental results demonstrate that the proposed method can improve the DSR performance remarkably in terms of EVM and ACPR, even when the PA operates in highly nonlinear states to ensure high drain efficiency. More complicated conditions (e.g., varying pressure, volume, temperature, and bandwidth) can be explored for future work.

References

[1] B. F. Beidas, "Adaptive digital signal predistortion for nonlinear communication systems using successive methods," *IEEE Trans. Commun.*, vol. 64, no. 5, pp. 2166–2175, May. 2016.

[2] Q. Wu, J. Jing, X.-W. Zhu, and C. Yu, "Digital predistortion for concurrent dual-band millimeter wave analog multibeam transmitters," *IEEE Trans. Circuits Syst., II, Exp. Briefs*, vol. 69, no. 3, pp. 1747–1751, Mar. 2022.

[3] K. J. Layton, A. Mehboob, A. Akhlaq, F. Bagaglini, W. G. Cowley, and G. Lechner, "Predistortion for wideband nonlinear satellite downlinks," *IEEE Commun. Lett.*, vol. 21, no. 9, pp. 1985–1988, Sep. 2017.

[4] B. Shi, "Digital predistortion linearization of wideband transmitter for high data rate satellite communications," in *2019 IEEE Asia-Pacific Microwave Conference (APMC)*, Dec. 2019, pp. 1589–1591.

[5] J. Zanen, E. Klumperink, and B. Nauta, "Power efficiency model for mimo transmitters including memory polynomial digital predistortion," *IEEE Trans. Circuits Syst., II, Exp. Briefs*, vol. 68, no. 4, pp. 1183–1187, Apr. 2021.

[6] P. L. Gilabert, D. López-Bueno, and G. Montoro, "Spectral weighting orthogonal matching pursuit algorithm for enhanced out-of-band digital predistortion linearization," *IEEE Trans. Circuits Syst., II, Exp. Briefs*, vol. 66, no. 7, pp. 1277–1281, Jul. 2019.

[7] Z. Alina and O. Amrani, "On digital post-distortion techniques," *IEEE Trans. Signal Process.*, vol. 64, no. 3, pp. 603–614, Feb. 2016.

[8] M. B. Salman and G. M. Guvensen, "An efficient QAM detector via nonlinear post-distortion based on FDE bank under PA impairments," *IEEE Trans. Commun.*, vol. 69, no. 10, pp. 7108–7120, Oct. 2021.

[9] M. Ben Mabrouk, G. Ferré, E. Grivel, and N. Deltimple, "A novel digital post-distortion and detection technique for RF power amplifiers in cognitive radio systems," in *2015 IEEE International Wireless Symposium (IWS 2015)*, Jul. 2015, pp. 1–4.

[10] A. Boudjemai, R. Hocine, and S. Guerionne, "Space environment effect on earth observation satellite instruments," in *2015 7th International Conference on Recent Advances in Space Technologies (RAST)*, 2015, pp. 627–634.

[11] J. Sun, J. Wang, L. Guo, J. Yang, and G. Gui, "Adaptive deep learning aided digital predistorter considering dynamic envelope," *IEEE Trans. Veh. Technol.*, vol. 69, no. 4, pp. 4487–4491, Apr. 2020.

[12] Y. Guo and A. Zhu, "Power adaptive decomposed vector rotation based digital predistortion for RF power amplifiers in dynamic power transmission," in *2017 IEEE Topical Conference on RF/Microwave Power Amplifiers for Radio and Wireless Applications (PAWR)*, Mar. 2017, pp. 8–10.

[13] Y. Zhang, Z. Wang, Y. Huang, W. Wei, G. F. Pedersen, and M. Shen, "A digital signal recovery technique using dnns for LEO satellite communication systems," *IEEE Trans. Ind. Electron.*, vol. 68, no. 7, pp. 6141–6151, Jul. 2021.

[14] X. Yu, X. Hu, Z. Liu, C. Wang, W. Wang, and F. M. Ghannouchi, "A method to select optimal deep neural network model for power amplifiers," *IEEE Microw. Wireless Compon. Lett*, vol. 31, no. 2, pp. 145–148, Feb. 2021.

[15] Z. Liu, X. Hu, L. Xu, W. Wang, and F. M. Ghannouchi, "Low computational complexity digital predistortion based on convolutional neural network for wideband power amplifiers," *IEEE Trans. Circuits Syst., II, Exp. Briefs*, vol. 69, no. 3, pp. 1702–1706, Mar. 2022.

[16] Q. Chen, Y. Zhang, F. Jalili, Z. Wang, Y. Huang, Y. Wang, Y. Liu, G. F. Pedersen, and M. Shen, "Robust digital signal recovery for LEO satellite communications subject to high SNR variation and transmitter memory effects," *IEEE Access*, vol. 9, pp. 135 803–135 815, Oct. 2021.

[17] J. Sun, W. Shi, Z. Yang, J. Yang, and G. Gui, "Behavioral modeling and linearization of wideband RF power amplifiers using BiLSTM networks for 5G wireless systems," *IEEE Trans. Veh. Technol.*, vol. 68, no. 11, pp. 10 348–10 356, Nov. 2019.

[18] A. Brihuega, L. Anttila, and M. Valkama, "Neural-network-based digital predistortion for active antenna arrays under load modulation," *IEEE Microw. Wireless Compon. Lett*, vol. 30, no. 8, pp. 843–846, Aug. 2020.

[19] Y. Yu, H. Yin, C. Yu, and J. Cai, "Polynomial-assisted neural network behavioral model of wideband radio frequency power amplifiers for 5g new radio," in *2020 IEEE MTT-S International Conference on Numerical Electromagnetic and Multiphysics Modeling and Optimization (NEMO)*, 2020, pp. 1–4.

[20] K. Hornik, "Approximation capabilities of multilayer feedforward networks," *Neural networks*, vol. 4, no. 2, pp. 251–257, 1991.

[21] CREE, *CGH40006, 6 W, GaN HEMT by cree for general purpose (CGH40006P) (wireless devices) transistor*, May. 2015.